Atmospheric Research 242 (2020) 105016

Contents lists available at ScienceDirect

Atmospheric Research

journal homepage: www.elsevier.com/locate/atmosres

Causes of the upper-level warm temperature anomaly (UWTA) associated with March–May heavy rainfall in Tanzania

Kantamla Biseke Mafuru[a,b,c,*], Tan Guirong[a,*]

[a] Key Laboratory of Meteorological Disaster, Ministry of Education (KLME), Joint International Research Laboratory of Climate and Environment Change (ILCBC), Collaborative Disasters (CIC-FEMD), Nanjing 210044, China
[b] College of Atmospheric Sciences, Nanjing University of Information Science and Technology, Nanjing, Jiangsu 210044, China
[c] Tanzania Meteorological Authority, Dar es Salaam, Tanzania

ARTICLE INFO

Keywords:
Upper-level warm temperature anomaly
Convective coupled Kelvin waves
Walker circulation
Heavy rainfall
Sea surface temperature

ABSTRACT

This study diagnoses the cause of the upper-level warm temperature anomaly (UWTA) associated with March–May (MAM) heavy rainfall of 1980–2010 in Tanzania in terms of the empirical orthogonal function (EOF), singular value decomposition (SVD) and dynamical diagnosis. EOF reveals the dominance of enhanced UWTA over the entire study region with strong warming to the northern coast, central, south-western highlands (SWH) and western part of the country. SVD depicts a monopole positive co-variability between the UWTA of the entire study area and SSTA over the entire domain of the Indian Ocean with strong positive coefficients to the central equatorial and western Indian Ocean (WIO). The lead-lag correlation coefficients between the three months running mean for the normalized WIO SSTA and UWTA indices show that, the UWTA formation starts early before MAM with the highest peak in February–April (FMA). The ascending branch of the Walker circulation is the dominant primer for the vertical uplift of warm moist air from the WIO during MAM while convective coupled Kelvin waves (CCKWs) dominate in FMA season. In both seasons, strong positive zonal temperature advection anomalies over the WIO spread towards the study area thereby dominating diabatic cooling and further increase the upper-level tropospheric temperature. Thus, diabatic heating due to enhanced uplift of warm and moist air from enhanced warm SSTA of the WIO warms the upper-level troposphere (i.e., also the UWTA) of the study area through the zonal temperature advection.

1. Introduction

Climate extremes related to excessive rainfall events over wide regions in African continent have brought into socio-economic consequences to millions of peoples' livelihood. A profound devastating impact is strongly observed on rain-fed agriculture, pastoralism (Verdin et al., 2005),water, food security (Viste et al., 2013; Verdin et al., 2005) and public health (Epstein, 1999). An improved forecast through a better understanding of the circulation anomalies responsible in producing the above average rainfall in the region is needed to reduce the severity of such outbreaks and ameliorate human suffering. Some studies have been carried out in Africa trying to relate the influence of the local forcing by sea surface temperature (SST) in the adjacent Atlantic and Indian Oceans together with a remote teleconnections from the tropical Pacific Ocean (Giannini, 2003). However, there are little information on the mechanism associated with the March–May (MAM) rainfall (long rain season) variability in East Africa (Camberlin and Philippon, 2002) and Tanzania in particular. Notably, some researchers (Cadet, 1985; Reverdin et al., 1986; Beltrando and Camberlin, 1993; Hastenrath et al., 1993; Mutai and Ward, 2000) have revealed that El-Niño Southern Oscillation (ENSO) has impacts on African's long rain. Specifically, the El-Niño Modoki events tend to induce significant rainfall enhancement over the northern tropical Eastern Africa during MAM season through anomalous changes in Walker circulation (Preethi et al., 2015). However, some early studies (Ogallo, 1988; Ogallo et al., 1988; Hastenrath et al., 1993; Rowell et al., 1994; Phillips and McIntyre, 2000) noted insignificant correlation between East Africa long rain season and either the atmospheric or oceanic component of ENSO based on different temporal and spatial scales. Some studies (i.e., Behera et al., 1999; Latif et al., 1999; Black et al., 2003; Hastenrath, 2007) showed a coherent association of the Indian Ocean dipole (IOD) with several flooding events across East African region. According to

* Corresponding author at: Key Laboratory of Meteorological Disaster, Ministry of Education (KLME), Joint International Research Laboratory of Climate and Environment Change (ILCBC), Collaborative Disasters (CIC-FEMD), Nanjing 210044, China.
E-mail addresses: kmafuru@gmail.com (K.B. Mafuru), tanguirong@nuist.edu.cn (T. Guirong).

https://doi.org/10.1016/j.atmosres.2020.105016
Received 25 February 2019; Received in revised form 20 April 2020; Accepted 27 April 2020
Available online 29 April 2020

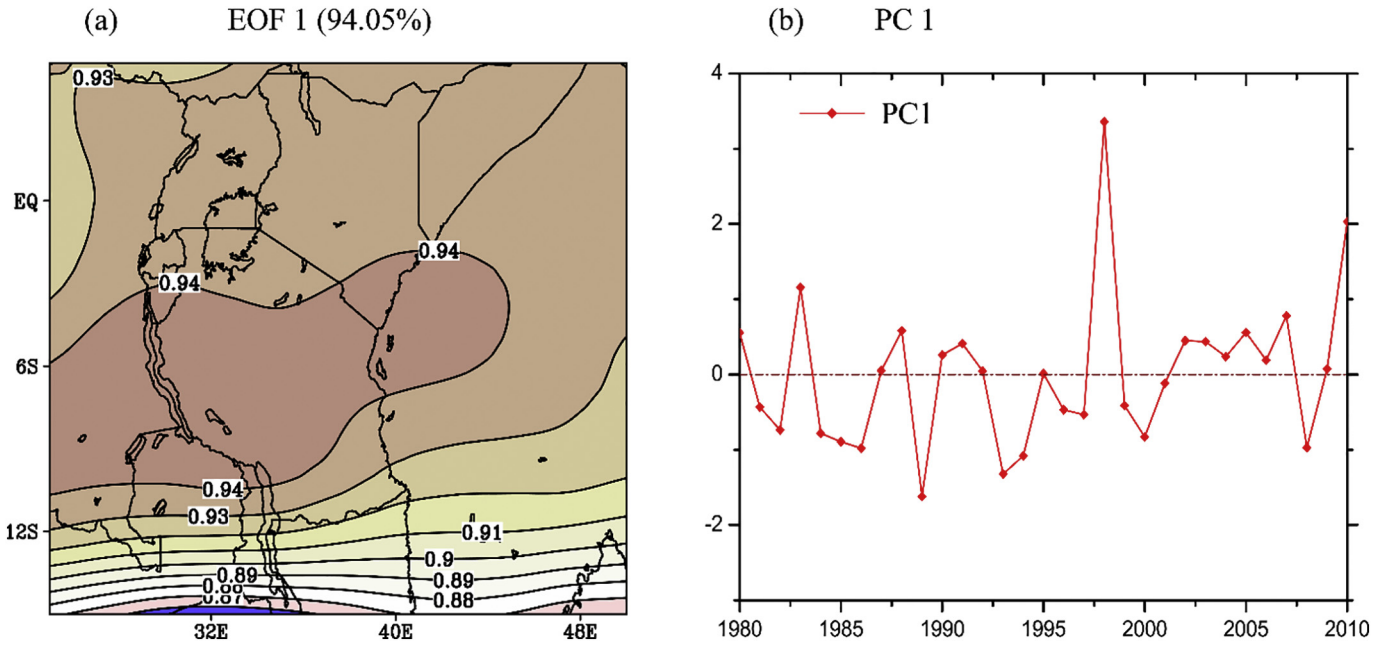

Fig. 1. (a) The spatial pattern of the first EOF mode (EOF1) and its corresponding principal component time series (PC1) in (b) of the mean 300-hPa temperature anomaly during MAM of 1980–2010.

Table 1
The squared covariance for the first two leading modes of a direct SVD expansion expressed in percentage and the temporal correlation coefficient between the expansion coefficients of the mean UWTA and SST anomalies, r (UWTA, SSTA) over the Indian Ocean during MAM of 1980 to 2010.

Mode	SCF (%)	r (UWTA, SSTA)	T300 Variance (%)	SST Variance (%)
1	99.89	0.9048	96.3	54.07
2	0.1	0.5220	2.02	4.18

Preethi et al. (2015), the positive IOD events are associated with enhanced rainfall activities over Eastern Africa through the anomalously strengthened tropical easterly jet stream. Notably, the co-occurrence of the canonical El-Niño Modoki and positive IOD may tend to induce strong anomalous enhancement in rainfall over the Eastern Africa region. The Indian Ocean can exert much more influence on rainfall near around in comparison with the rest Oceans (Fang et al., 2017, 2018; Ummenhofer et al., 2009). Goddard and Graham (1999) related SST, moisture flux and wind circulation patterns with rainfall over East Africa. The basin-wide warming in the Indian Ocean is associated with significant enhancement of rainfall over the northern tropical Eastern Africa (Preethi et al., 2015). Okoola (1989) and Hills (1978) found the existing relationship between wind circulation patterns and rainfall over East Africa. On the other hand, Camberlin and Philippon (2002) noted the positive correlation in extra-tropical south-west Atlantic Ocean towards the end of the long rain and more extensively in the equatorial Indian Ocean. Rowell et al. (1994) found that; a poor or late start of the MAM season is connected with a cool tropical North Atlantic. It's clear that, afore mentioned research findings put more emphasis on the impact of surface/low-level circulation anomalies but still a gap exists in ascertaining any strong and robust atmospheric or oceanic forcing of the East African long rain season.

In our recent study (i.e., Mafuru and Guirong, 2018) trying to assess the upper-level warm temperature anomaly (UWTA, in hereafter the 300-hPa warm temperature anomaly) and its impact on prone areas to heavy rainfall during MAM season in Tanzania, we found that, the UWTA has a direct influence/impact on MAM heavy rainfall. It influences the (1) formation of upper-level horizontal wind divergence (2) strengthening the upper-level westerly winds (3) formation of the low-pressure cell at low levels. The overall effect is towards accelerating vertical ascent, deepening the surface low pressure for enhanced convective processes and heavy rainfall events (HREs) formation over the northern sector of Tanzania which was mostly affected. Few studies have embarked on the linkage existing between the UWTA and the severity of climate anomalies worldwide. On their work (Jiang et al., 2013) to investigate the variation and predictability of the winter time upper-tropospheric temperature (UTT) over Asia, they realized an often linkage of the UTT with severe climate anomalies and associated features of large scale circulation and surface climate. Meanwhile, Zhang and Zhou (2012) reported that the upper-level tropospheric warm anomaly reinforces the formation of an anticyclonic (cyclonic) anomaly above (below) most areas in northern China. The major feature of the event was towards strengthening (weakening) westerly winds to the North (South) of the warm center pushing the high-level westerly jet to the North. Consistently, the cyclonic anomaly deepens the trough upstream of central northern China and intensifies lower south-westerly winds to the mid-East of the warm center. As a result, the northerly stretched high-level jet produces the upper-level divergence in its right-front side while the intensified south-westerly winds induce lower moisture convergence in its left-front side fostering heavy rainfall in central northern China.

Given the important roles and previous devoted works on the characteristic mechanisms of the UWTA but still further research on the dynamics and its sources remain uncertain. To bridge this gap, the current study focuses on the inter-annual variation of the UWTA in Tanzania associated with HREs of the 1980–2010 MAM rainfall season aiming at (1) identifying distinct modes of inter-annual variation of UWTA (2) ascertaining the circulation anomalies associated with the dominant modes of variability which on the other hand stand as the sources of the UWTA. The remainder of the paper is organized as follows: Descriptions of data and analysis methods are given in section 2. The dominant modes of the inter-annual variations and the circulation anomalies associated with the UWTA are discussed in section 3. In section 4, we provide the summary and conclusion of the results obtained.

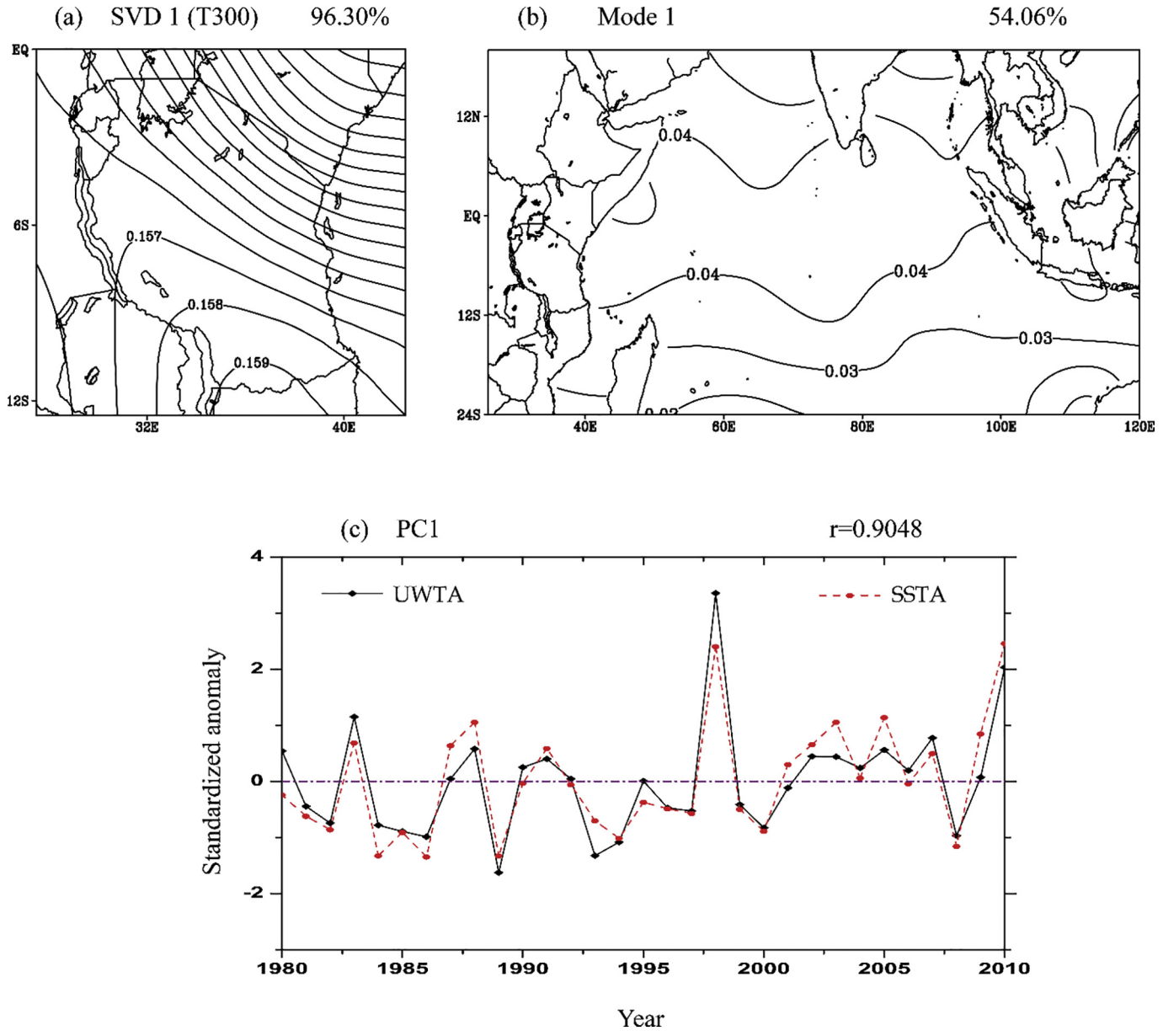

Fig. 2. Loading maps for the first SVD modes of the (a) 300-hPa temperature anomaly (b) SSTA over the Indian Ocean and its corresponding temporal amplitudes of the principal component time series in (c). The fractions of variance of the normalized data field explained by the respective modes are indicated in the right-hand corner of each map.

2. Data and methodology

2.1. Data description

The National Centers for Environmental Prediction-National Center for Atmospheric Research (NCEP-NCAR) monthly mean reanalysis datasets from 1949 to present (Kalnay et al., 1996) provide a gridded analysis of the global observational network of meteorological variables (i.e. temperature, wind, vertical velocity and velocity potential) that were used in this study. The data spans with a spatial resolution of 2.5°X2.5° grid at every 6 h. The monthly mean sea surface temperature data were obtained from the National Oceanic and Atmospheric Administration (NOAA) with a 2.0° latitude-longitude resolution (Smith et al., 2008). The characteristics for convective processes are studied based on the outgoing long wave radiation (OLR) in a similar manner to Wheeler and Kiladis (1999). The NOAA daily mean OLR data sets (Liebmann and Smith, 1996) were used as the proxy for deep tropical convection and are interpolated onto 2.5°X2.5° gridded maps. The data sets span from 1974 to 2017 and are interpolated in time and space twice daily OLR values and averaged to once daily.

2.2. Methodology

In this study singular value decomposition (SVD) was used to analyze the large scale inter-annual variability between the 300-hPa temperature anomalies (T300) in Tanzania and the sea surface temperature anomalies (SSTA) over the Indian Ocean during MAM rainfall season of 1980 to 2010. The aim was to ascertain the possible existing relationship between the two. SVD involves the matrix operation applied to covariance between grid point observations of two fields. It therefore decomposes the matrix of two fields into singular values with two sets of paired-orthogonal vectors namely the loading maps. A detailed discussion on SVD and its application to idealized and observed data, kindly refer to Bretherton et al. (1992). However, the empirical

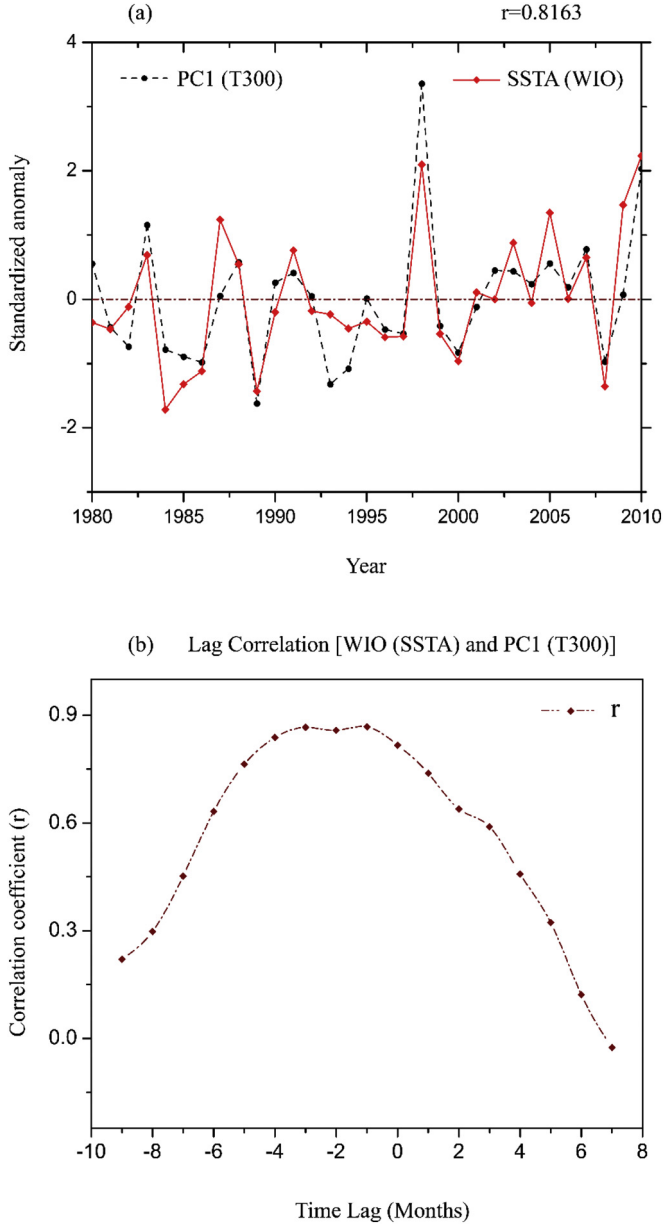

Fig. 3. (a) The time series correlation coefficient between PC1 for EOF1 and normalized SST anomalies over the western Indian Ocean (WIO, 38°E-78°E, 20°S-3°N) (b) The lead-lag correlation coefficients between the three months running mean (i.e. 3-month means stepped one month at times) normalized SST anomalies depicted over the WIO and UWTA indices during MAM of 1980–2010. The month (−1) shows that SSTA indices lag the UWTA indices by one month (i.e. FMA) while month (0) shows the two are in phase during the current MAM season. Meanwhile, month (+1) denotes that SSTA indices lead the UWTA indices by one month (i.e. June–August, JJA).

orthogonal function (EOF) was carried on the mean MAM T300 averaged over the domain bounded by 20°E-50°E and 15°S-5°N. EOF analysis is frequently applied to derive patterns and indexes used to identify and track weather and climate modes as expressed in state variables or proxies of convection (Roundy, 2015). It aims at extracting the leading climatic modes which will further mark prone areas associated with enhanced UWTA during the season. Meanwhile, in the analysis trying to elucidate the co-variability of the MAM convective coupled Kelvin waves (CCKWs) and the UWTA, we correlate the global tropical Kelvin filtered OLR anomalies and the first principal component time series (PC1) of the first EOF mode (EOF1). The wave-number frequency filtering for the 31 years OLR time series has been carried out in this study following the method deployed by Wheeler and Kiladis (1999). We first filter the Kelvin wave within the period of 2.5-17 days and an eastward wave number 1–14 similar to Straub and Kiladis (2002) and later we average the daily filtered Kelvin OLR into monthly means. Exceptionally, assessing the effect of the latent heat released following vertical ascent of the moist air from warm tropical Indian Ocean we first calculate the three dimensional (3D) diabatic heating, $\overline{Q_1}$ diagnosed as a residual in the thermodynamic equation (Hoskins et al., 1989; Nigam, 1994) and there after we computed the composite analysis for the field. The 3D diabatic heating, $\overline{Q_1}$ computational is as follows;

$$\overline{Q_1} = \frac{\partial \overline{T}}{\partial t} + \overline{\boldsymbol{V}}.\nabla\overline{T} + \left(p/p_o\right)^{R/C_p}\overline{\omega}\frac{\partial\overline{\theta}}{\partial p} + \left(p/p_o\right)^{R/C_p}\left[\nabla.\overline{V\theta} + \frac{\partial(\overline{\omega\theta})}{\partial P}\right] \quad (1)$$

Where V, ω, T and θ are the 3D horizontal velocities, temperature and potential temperature while R and C_p are the gas constant and specific heat at constant pressure of dry air and $p_o = 1000\ hPa$. The overbar represents the monthly average of the reanalysis field. The terms in the right of Eq. (1) stands for local temperature change, horizontal temperature advection, adiabatic heating and transient eddy heating respectively (Yanai and Li, 1994; Tamura et al., 2010). The composites products were later subjected to a two tailed Student's *t*-test to validate their significance (Indeje et al., 2000). In addition, correlation and composite analysis are used in this study.

3. Results and discussion

3.1. Prone areas to UWTA and its relation with the Indian Ocean SST anomalies

Fig. 1a display eigenvectors of covariance matrices of EOF1 and its corresponding principal component time series (Fig. 1b) among the three leading EOF modes of co-variability for the 300-hPa mean temperature anomalies during MAM of 1980 to 2010. The first three EOF patterns explain more than 98.16% of the total variance and therefore being more representative of the country's seasonal UWTA distribution. The fist EOF (Fig. 1a) accounts for 94.05% of the total variance for the entire season while EOF2 and EOF3 (i.e., figures not included in this study) only accounts for 2.84% and 1.27% respectively. EOF1 (Fig. 1a) exhibit a monopole mode of variability with positive loadings over the entire study region while the highest weight of positive eigenvector coefficients concentrates over the northern coast, central, south-western highlands (SWH) and western part of the country. Notably, PC1 of the first EOF is assigned to represent the UWTA index for further analysis. The spatial relationship between the UWTA and the Indian Ocean SSTA is assessed with the SVD analysis. Table 1 summarizes the results for the first two leading modes in SVD expansion of the mean UWTA and SST anomalies over the Indian Ocean. The squared covariance fraction (SCF) results in Table 1 strongly concentrate in the first two modes and account for about 99.91% of the total squared covariance. The corresponding fractions of the variances for the UWTA and Indian SSTA fields explained by the time series of the expansion coefficient component are 98.32% and 54.25% respectively. Generally, the expansion coefficients for both modes as indicators in strength of coupling, exhibit correlation coefficients of greater than 0.5 (see Table 1). It is clear from these statistics (Table 1) to signify how important the first two modes are in explaining the association between UWTA and Indian SSTA variability in Tanzania during MAM rainfall season.

The first SVD (in hereafter SVD1) coupled modes (Figs. 2a and b) that dominate the co-variability between the March–May UWTA and SSTA over the Indian Ocean, reveal a monopole positive co-variability between T300 over the entire study area (Fig. 2a) and SSTA over the entire domain of the Indian Ocean (Fig. 2b) with strong positive coefficients being to the central equatorial and western Indian Ocean. Exploring further the coupling strength of association between SSTA over the WIO and the UWTA during MAM season, we correlate the

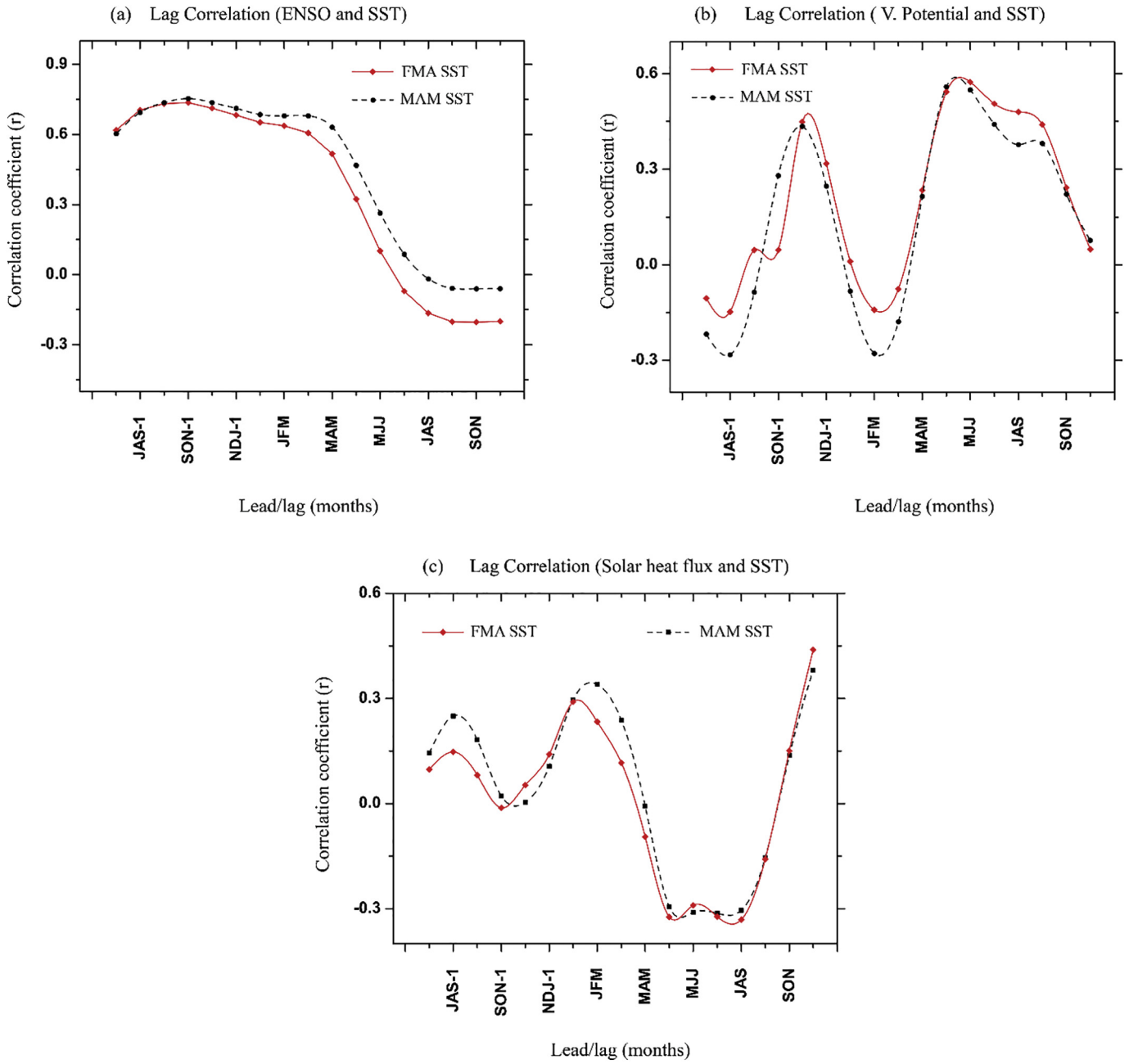

Fig. 4. The lead-lag correlation coefficients between the three months running mean (i.e. 3-month means stepped one month at times) normalized SST anomalies depicted over the western Indian Ocean [WIO (38°E-78°E, 20°S-3°N) and (a) ENSO indices (b) 850 hPa velocity potential indices (c) net solar heat flux indices during both FMA and MAM seasons of 1980–2010. The month (−1) shows that SSTA indices lag the UWTA indices by one month (i.e. FMA) while month (0) shows the two are in phase during the current MAM season. Meanwhile, month (+1) denotes that SSTA indices lead the UWTA indices by one month (i.e. June–August, JJA).

standardized SSTA from the WIO (an area bounded with 38°E-78°E and 20°S-3°N) and the UWTA index (i.e. PC1). Fig. 3a shows the time series correlation between PC1 of the first EOF and SSTA over the WIO. The results reveal the presence of strong positive correlation ($r > 0.8$) which is statistically significant at 5% levels with a two tailed student's *t*-test. Since the coupling association indicates a robust positive correlation, it suggests that the WIO has important signal of variability for the UWTA formation during MAM season. Assessing the existing relation between the UWTA and SSTA over the WIO before, during and after MAM season, we conducted a lead-lag correlation between the three months running mean of the normalized WIO SSTA and UWTA indices. The lead-lag correlation results are shown in Fig. 3b in which month (−1) shows that SSTA indices lag the UWTA indices by one month (i.e. FMA) while month (0) showing the two are in phase during the current MAM season. Meanwhile, month (+1) denotes that SSTA leads the UWTA indices by one month (i.e. June–August, JJA).

Fig. 3b depicts a simultaneous statistically significant increase in correlation over the WIO from August–October (ASO) of the previous year to the current FMA season where it attains the highest peak ($r = 0.8677$) then decreasing afterwards. The highest peak in correlation depicted in Fig. 3b reflect that, the UWTA generation through enhanced SSTA over the WIO starts early before MAM with the highest peak being in FMA. In view of that, the present study advances the analysis in FMA season trying to validate on how the leading SSTA over the Indian Ocean influence the formation of the UWTA.

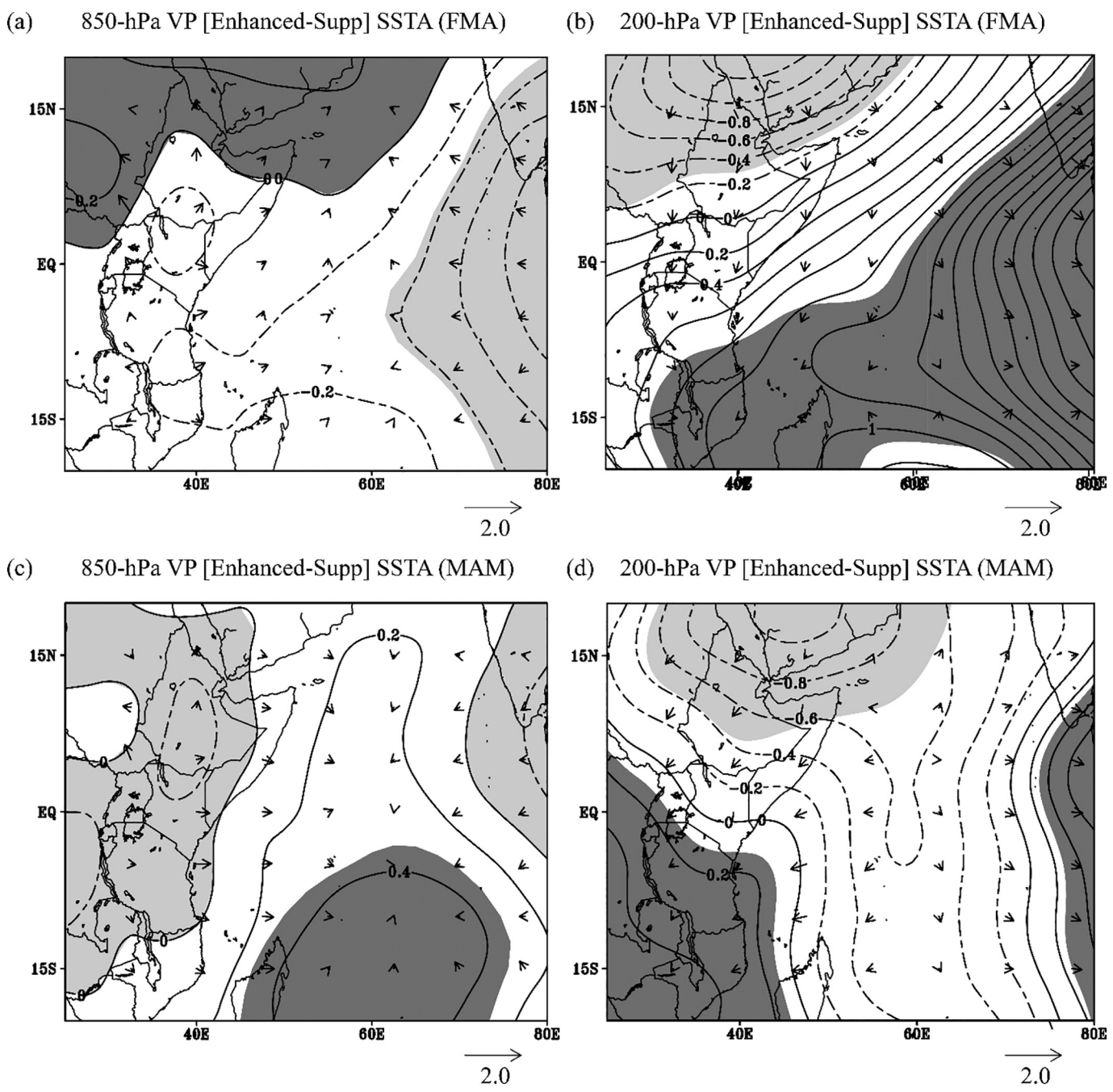

Fig. 5. The composite pattern for the velocity potential ($10^6 m^2 s^{-1}$) and divergent wind (ms^{-1}) anomalies for the difference between enhanced and suppressed SSTA at (a) 850-hPa (b) 200-hPa during FMA while in (c) 850-hPa and (d) 200-hPa during MAM season of 1980 to 2010. The shaded areas are statistically significant at 5% level with a two tailed Student's *t*-test.

3.2. Relative influence of SSTA over the Indian Ocean to the formation of the UWTA

To explore the influence of SSTA over the WIO on the UWTA formation during FMA (i.e., the leading influence) and MAM seasons, we carried out the difference composite analysis of the number of field variables over the WIO. The composite involves the difference between years with enhanced and suppressed SSTA trying to demonstrate the mechanism influenced by SSTA on the UWTA formation. Based on principal component time series of SVD1 for the SSTA expansion, years with strong amplitude of normalized mean MAM SST departures of $\geq +1$of the standard deviation (1988, 1998, 2003, 2005, and 2010) and those ones with strong amplitudes of normalized departures of ≤ -1 of the standard deviation (1984, 1986, 1989, 1994, 2008) were selected as enhanced and suppressed SSTA years respectively. The composite spatial pattern for the SSTA associated with enhanced SSTA over the WIO during FMA and MAM seasons (figures not included) strongly resembles the spatial pattern of the first SVD leading mode. The figures reveal warm SSTA over the entire Indian Ocean with strong positive coefficients over the western (i.e., 38°E-78°E, 20°S-3°N, here after WIO). Interestingly, the results showed much stronger warm SSTA over the WIO during FMA season than in MAM season especially over the central and extreme north-eastern part of the WIO.

Examining the possible evolution of the enhanced warm SST over the WIO, we performed a lead/lag correlation for the normalized SSTA over the WIO and some of the atmospheric variables (i.e., velocity

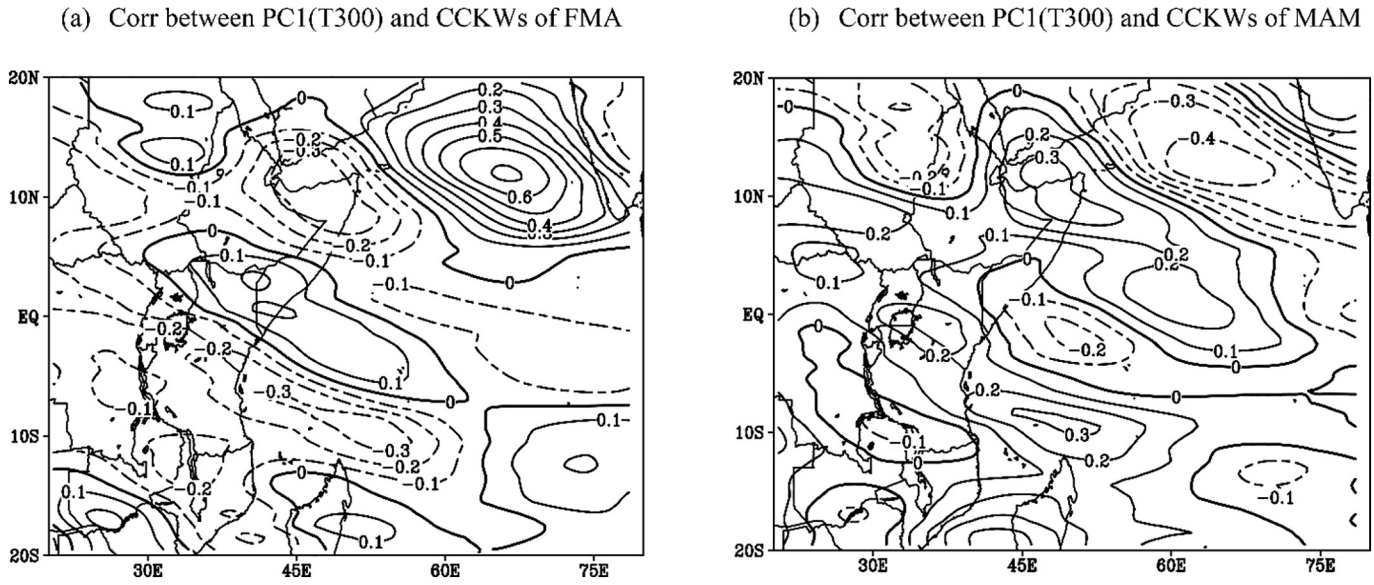

Fig. 6. The spatial pattern for the correlation between the Kelvin filtered OLR variance anomalies and SSTA (i.e. PC1 obtained from EOF1 in Fig. 1b) during (a) FMA (b) MAM seasons of 1980–2010. The positive correlations are represented by solid line while negative correlations are in dashed lines.

potential and net solar heat flux indices). These indices were computed as the normalized average from the WIO. As observed in Fig. 4a, it is apparent that the SSTA over the WIO during FMA and MAM reveals a strong positive correlation (i.e., $r = 0.7365$ in FMA and 0.7541 in MAM) with ENSO indices of the previous SON. This indicates that warm phase of ENSO during SON of the central equatorial Pacific has important signal of variability for the enhanced warm SST over the WIO the following MAM. However, the moderate positive correlation between the 850 hPa velocity potential and SSTA of the WIO during the previous OND (Fig. 4b) shows the presence of an altered Walker circulation with anomalous rising over the WIO, central and eastern equatorial Pacific while anomalous sinking to the western equatorial Pacific and Indonesian Archipelago. In our recent study (Mafuru and Tan, 2019) we have stated that, the anomalous sinking to the western equatorial Pacific and Indonesian Archipelago during warm phase of ENSO of the previous SON coincides with suppression in total clouds. It therefore fosters the increase in total net heat solar flux absorbed by the Ocean leading into enhanced warm SSTA. The presence of the well-organized/strengthened easterly wind flow from the central and north western Pacific and Indonesian Archipelago to tropical Indian Ocean from the previous SON to the following MAM, spread the warm SSTA to the WIO. The current January to March (JFM) in Fig. 4c reveals enhanced solar heat flux over the WIO following the positioning of the descending limb of the Walker circulation to the WIO. It is the descending limb of the Walker circulation which suppresses cloud cover while favors the increase in net heat flux absorbed by the Ocean.

It is worth noting that warm sea surface temperature has a significant impact on organized tropical convection associated with atmospheric convergence/divergence and vertical motion (Graham and Barnett, 1987). In this study we therefore show that, enhanced SSTA over the WIO is accompanied by the adjacent Walker and vertical motion. Fig. 5 represents the composite velocity potential and divergent/convergent wind anomalies for the differences between enhanced and suppressed SSTA during FMA and MAM seasons of 1980 to 2010. The centers of low (high) velocity potential are associated with divergent outflow (confluent inflow) of winds. Meanwhile, divergence (convergence) in the upper-level troposphere (i.e., 200-hPa) is accompanied with convergence (divergence) in the lower troposphere. During MAM season (Fig. 5c) the WIO is clearly seen marked with the low tropospheric convergence with the center of convergence (i.e. at 60°E) over the region occupied by strong enhanced warm SSTA. The positive velocity potential and wind convergence over WIO in Fig. 5c at low level coupled the upper-level negative velocity potential and tropospheric wind divergence (Fig. 5d). It therefore reflects the position of the ascending limb of the local Indian Ocean Walker circulation over East Africa which enhances convection due to enhanced uplift. However, during FMA season we noticed the intrusion of the negative velocity potential and wind divergence at lower level (Fig. 5a) for the area occupied by enhanced warm SSTA over the WIO. This area is accompanied by positive velocity potential (Fig. 5b) in the upper-level thereby signifying the weakening of the rising limb of the Walker circulation a month earlier (i.e., in FMA).

Assessing the source of vertical uplift over the WIO during FMA season, we expanded our findings trying to analyze whether there is an existing association between the CCKWs and the UWTA formation. Some researchers have related the enhanced convection and the CCKWs propagation. For instance, Nguyen and Duvel (2008) demonstrated a close relationship between convection and CCKWs activities following their study of the equatorial African convection. Roundy (2008) on the other hand noted that, CCKWs propagate through Africa into Indian Ocean raises the intriguing possibility that processes operating over tropical Africa may influence the nature and predictability of convection in the equatorial Indian Ocean. Having noted these research findings, we carried the correlation analysis between the Kelvin filtered OLR anomalies over the tropical Indian Ocean and PC1 of the first EOF mode for the 300-hPa temperature anomalies during both FMA and MAM seasons.

Fig. 6a shows a relatively strong positive correlation ($r > 0.6$) over the northern tropical Indian Ocean averaged over the region bounded by 60°E to 78°E. The higher the correlation between the two field variables show that there is strong in phase relationship between the warm SSTA over that region and CCKWs, and thus the enhanced warm SSTA region coincides with the active convection. It also suggests a favorable background environment for CCKWs propagation while the warming over the Indian Ocean being the precursor for the enhanced latent heat in the upper-level troposphere. Since the CCKWs are associated with enhanced convection and moisture convergence (Wheeler et al., 2000), the location of the CCKWs activities over the tropical Indian Ocean in Fig. 6a suggest a significant ascent of warm and moist air from the peak domain of the WIO. During MAM season we noticed the weak positive correlation between the Kelvin filtered OLR anomalies and PC1 of the first EOF mode for the 300-hPa temperature

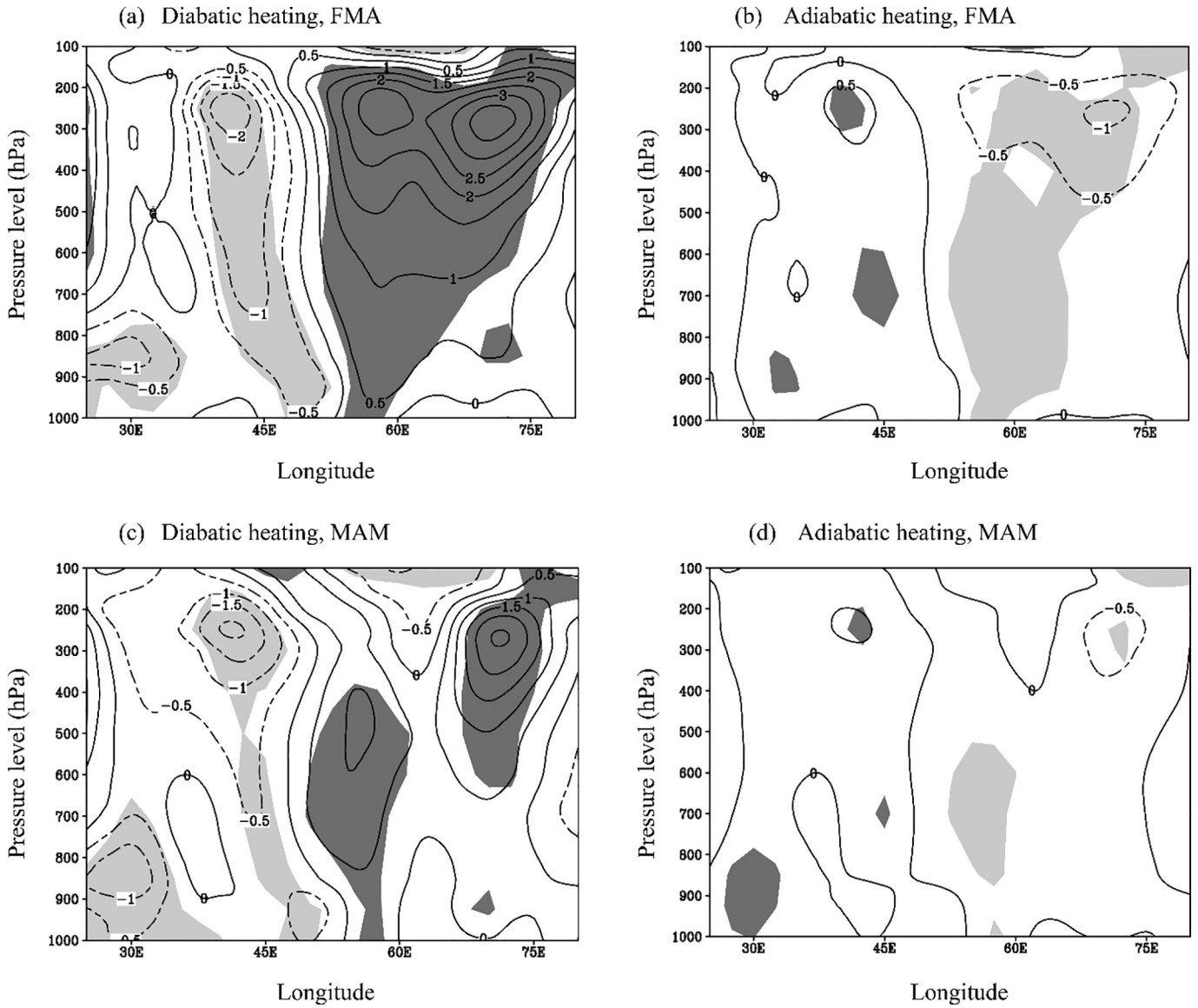

Fig. 7. The composite vertical cross-section anomaly distribution fields for the difference between enhanced and suppressed SSTA for the (a, c) diabatic heating anomalies (K day^{-1}) and (b, d) adiabatic heating (Kday^{-1}) along 20°S during (a, b) FMA and (c, d) MAM seasons of 1980–2010. The positive and negative values in (a-d) indicate adiabatic/diabatic warming and cooling respectively. The shaded areas are statistically significant at 5% level with a two tailed Student's t-test.

anomalies over the equatorial and tropical Indian Ocean (Fig. 6b). The scenario shows that, CCKWs activities are stronger (weaker) during FMA (MAM) season and the CCKWs being the dominant primer for the vertical uplift over the enhanced warm SSTA region of the WIO during FMA while ascending limb of the Walker circulation during MAM season.

3.3. The mechanism of the UWTA formation

A number of researchers have sighted clearly the process by which the parcel of air gains heat through the release of latent heat of condensation following its ascent. For instance, Lindzen and Nigam (1987), and Raymond (1994) pointed that, tropical SST anomaly (e.g. enhanced SSTA) tends to increase low level convergence and moisture thereby promoting enhanced deep convection and hence diabatic heating. However, Jiang et al. (2011) noted that, the latent heat release in tropics which is associated with deep convection is the dominant component of total diabatic heating and can further influence convection by modifying atmospheric instability through redistributing the localized latent heat and moisture or through dynamical lifting by low-level convergence. Taking into account the large ascent of warm moist air from an area occupied with enhanced warm SSTA over the WIO, we decided to compute both the adiabatic and diabatic heating and validate if the ascent is associated with the release of latent heat.

As shown in Fig. 7a and Fig. 7c, during FMA and MAM seasons, the broad region of the mid to higher level (600–200 hPa) of the warm SST over the WIO occupies stronger diabatic warming in comparison to weaker adiabatic cooling (Figs. 7b and d) following the enhanced uplift. Meanwhile, the spatial distribution of the adiabatic and diabatic heating also confirms the dominance of enhanced diabatic warming (Figs. 8a and c) over the WIO in comparison to less weak adiabatic cooling (Figs. 8b and d) during both FMA and MAM.

Fig. 9 shows the composite vertical cross-section anomaly distribution fields for the difference between enhanced and suppressed SSTA zonal-vertical circulation and diabatic heating anomalies during FMA and MAM seasons of 1980 to 2010. During MAM season (Fig. 9b), a significant updraft extending from low to higher level is observed over the region bounded by 50°E to 75°E (i.e., the region with enhanced warm SSTA). In the upper-level troposphere (i.e., 300–200-hPa) the ascent turns left thereby advecting the warm air towards the study

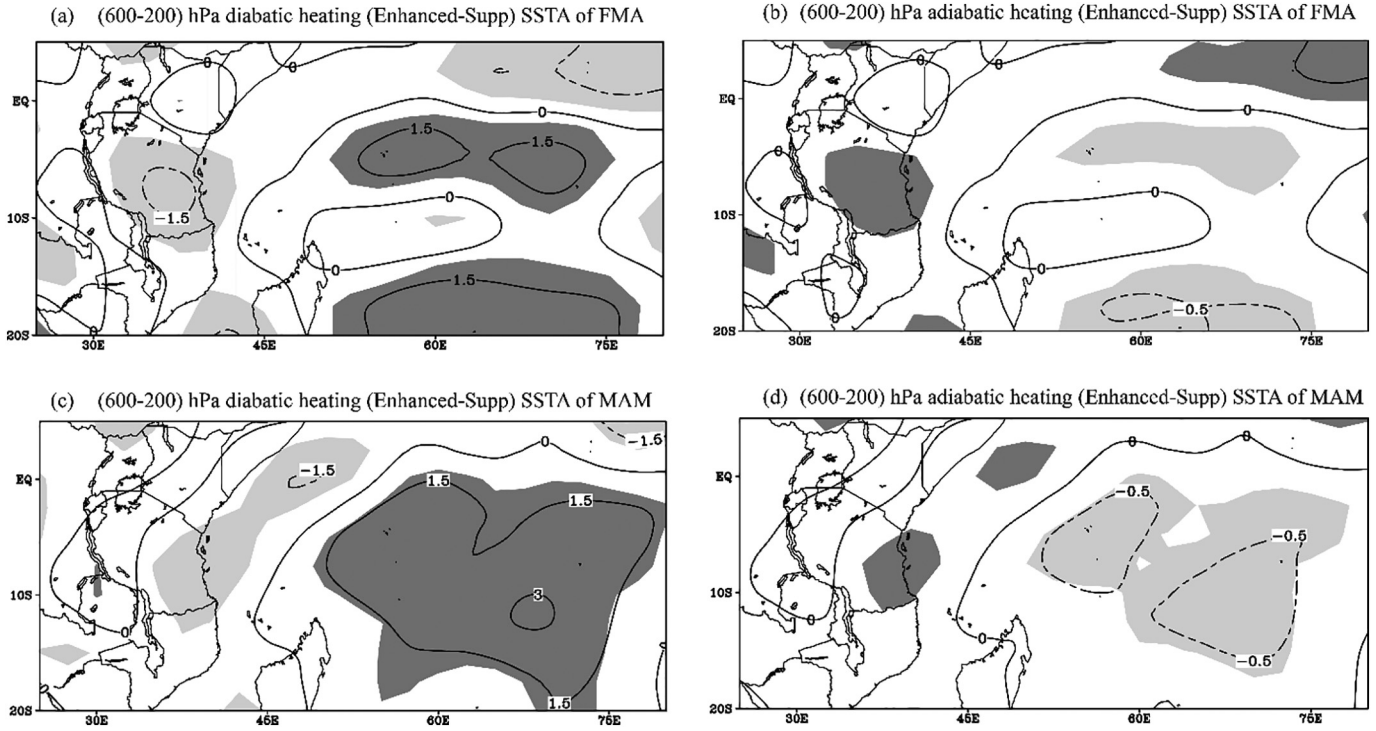

Fig. 8. The composite pattern for the 600–200-hPa mean (a, c) diabatic heating anomaly (K day^{-1}) and (b, d) adiabatic heating anomaly (K day^{-1}) distribution fields for the difference between enhanced and suppressed SSTA during (a, b) FMA and (b, d) MAM seasons of 1980–201. The positive and negative values in (a-d) indicate adiabatic/diabatic warming and cooling respectively. The shaded areas are statistically significant at 5% level with a two tailed Student's t-test.

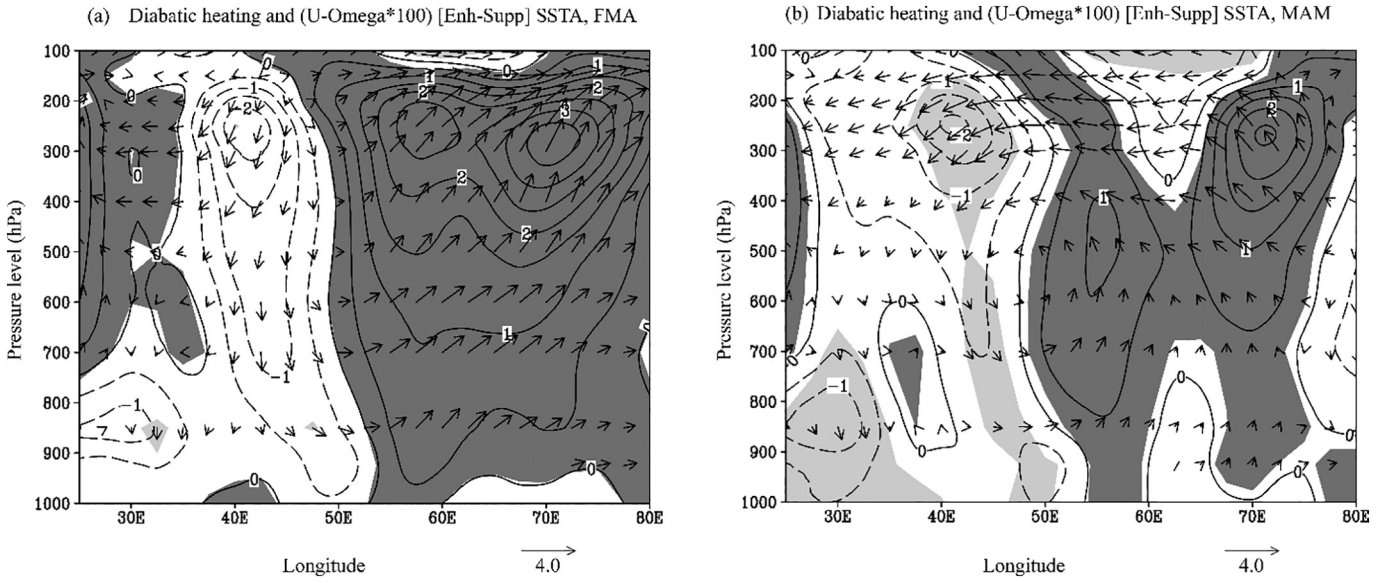

Fig. 9. The composite vertical cross-section anomaly distribution fields for the difference between enhanced and suppressed SSTA for the zonal-vertical circulation [hPa] (in vectors) and diabatic heating anomalies (K day^{-1}, in contour lines) obtained by averaging the divergent wind and vertical velocity along 20°S during (a) FMA (b) MAM seasons of 1980–2010. The positive and negative values in (a) and (b) indicate diabatic warming and cooling respectively. The shaded areas are statistically significant at 5% level with a two tailed Student's t-test.

region. The region occupied by the updraft over the WIO in Fig. 9b corresponds with significant diabatic heating which becomes stronger from the mid to higher level (i.e., 600–200-hPa). Indisputably, it is noted that strong (weak) mid to high level mean diabatic heating anomalies over the WIO (study region) corresponds with strong updraft (downdraft) observed in Fig. 9b.

However, during FMA season (Fig. 9a) the region of strong updraft (i.e., enhanced warm SSTA over the WIO) reveals a robust enhanced diabatic warming in the mid to higher level in comparison to MAM season. It therefore being in agreement with our earlier finding that the peak for the UWTA generation is one month before MAM season. On the other hand, the strong mean 600–200-hPa diabatic warming during FMA season concentrates over the extreme southern part of the WIO and tallies with the region with both enhanced SSTA and uplift.

Further, zonal temperature advection anomaly is analyzed for enhanced SSTA years during FMA and MAM seasons aiming at assessing if the accumulated diabatic warming over the mid and upper-level is advected to the study area. Fig. 10 shows the spatial pattern for the

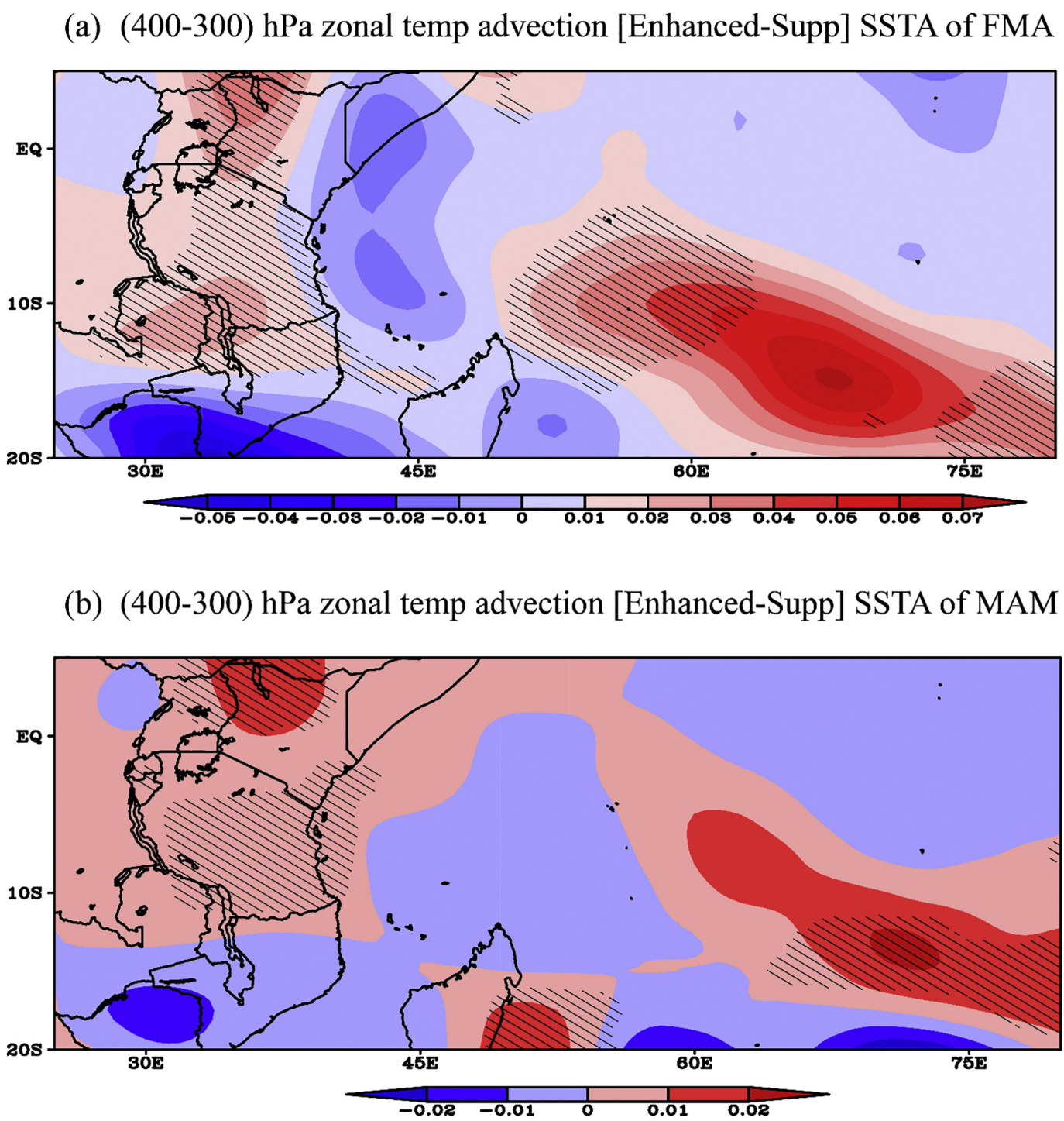

Fig. 10. The composite pattern for the 400–300-hPa mean zonal temperature advection anomalies $(-\overline{u}\partial\overline{T}/\partial x)'$ distribution fields for the difference between enhanced and suppressed SSTA during (a) FMA (b) MAM seasons of 1980–201. The hatched areas are statistically significant at 5% level with a two tailed Student's t-test.

400–300-hPa mean zonal temperature advection anomaly distribution fields for the difference between enhanced and suppressed SSTA during FMA and MAM seasons. There are stronger positive zonal temperature advection anomalies (Fig. 10a) over the extreme southern region of the WIO in FMA compared to MAM season (Fig. 10b) which is in correspondence with strong diabatic warming in the mid to high level. In both seasons the area of strong positive zonal temperature advection anomalies over the WIO spreads towards the study area (Figs. 10a and b). In this case, the warm zonal temperature advection anomalies dominate diabatic cooling over the study area and therefore increases the upper-level tropospheric temperature (i.e., increases the 300-hPa temperature anomaly). With this phenomenon we can deduce the fact that, diabatic heating due to enhanced uplift of warm and moist air from enhanced warm SSTA of the WIO warms the upper-level troposphere (i.e., also the UWTA) of the study area through the zonal temperature advection.

4. Summary and conclusion

The cause of the UWTA associated with MAM heavy rainfall in Tanzania during the 1980–2010 time span is extensively investigated in terms of EOF, SVD and dynamical diagnosis. The first EOF mode reveals

the occurrence of enhanced UWTA over the entire study region with strong warming over the northern coast, central, south-western highlands (SWH) and western part of the country. However, the first two SVD modes of variability account for about 99.91% % of the total squared covariance thereby signifying how important the modes are in explaining the association between the UWTA in Tanzania and SSTA over the Indian Ocean during MAM season. The first SVD coupled modes that dominate the co-variability between the March–May UWTA and the SSTA over the Indian Ocean, reveal a monopole positive co-variability between T300 over the entire study area and SSTA over the entire domain of the Indian Ocean with strong positive coefficients being to the central equatorial and western Indian Ocean.

The lead-lag correlation coefficient between the three months running mean of the normalized WIO SSTA and UWTA indices shows a simultaneous statistically significant increase in correlation from August–October (ASO) of the previous year to the current FMA season where it attains the highest peak ($r = 0.8677$) then decreasing afterwards. It therefore reflects the fact that, the UWTA formation starts early before MAM season and reaches the highest peak in the current FMA season. The region of enhanced SSTA over the WIO during FMA and MAM seasons tied with strong updraft, corresponds with significant diabatic heating which becomes stronger from the mid to higher level (i.e., 600–200-hPa). However, there is enhanced SSTA and mid to high level mean diabatic heating anomalies over the WIO during FMA than in MAM season which is in consistence with the region of strong updraft.

There is a relatively strong positive correlation ($r > 0.6$) between the Kelvin filtered OLR anomalies over the tropical Indian Ocean and UWTA during FMA season over the northern tropical Indian Ocean averaged over the region bounded by 60°E to 78°E which weaken in MAM season. On contrary, the rising limb of the Walker circulation over the region occupied by enhanced SSTA of the WIO weaken in FMA season while strengthened during MAM season. In this case we noticed that, the ascending branch of the Walker circulation is the dominant primer for the vertical uplift of warm moist air from the region of enhanced warm SSTA of the WIO during MAM while CCKWs dominate in FMA season. In both seasons the area of strong positive zonal temperature advection anomalies over the WIO spread towards the study area. Thus, the warm zonal temperature advection anomalies dominate diabatic cooling over the study area and therefore increase the upper-level tropospheric temperature (i.e., increases the 300-hPa temperature anomaly). With this phenomenon we can deduce that, diabatic heating due to enhanced uplift of warm and moist air from enhanced warm SSTA of the WIO warms the upper-level troposphere (i.e., also the UWTA) of the study area through the zonal temperature advection.

Declaration of Competing Interest

The authors declare that there is no potential conflict of interest whatsoever.

Acknowledgement

The authors wish to express their sincere thanks to NCEP/NCAR for making reanalysis data available. The first author is grateful to Nanjing University of Information Sciences and Technology (NUIST) for granting him the fellowship to pursue his PhD studies, without which this work could not have been possible. The work described in this paper is supported by National Key Research and Development Program of China (2018YFC1505804), and National Natural Science Foundation of China (41575070, 41575085).

References

Behera, S.K., Krishnan, R., Yamagata, T., 1999. Unusual Ocean-atmosphere conditions in the tropical Indian Ocean during 1994. Geophys. Res. Lett. 26, 3001–3004. https://doi.org/10.1029/1999GL010434.

Beltrando, G., Camberlin, P., 1993. Interannual variability of rainfall in the eastern horn of Africa and indicators of atmospheric circulation. Int. J. Climatol. 13, 533–546. https://doi.org/10.1002/joc.3370130505.

Black, E., Slingo, J.M., Sperber, K.R., 2003. An observational study of the relationship between excessively strong short rains in coastal East Africa and Indian Ocean SST. Mon. Weather Rev. 74–94. https://doi.org/10.1175/1520-0493(2003)131<0074:AOSOTR>2.0.CO;2.

Bretherton, C.S., Smith, C., Wallace, J.M., 1992. An Intercomparison of Methods for Finding coupled patterns in climate Data. J. Clim. 5, 541–560. https://doi.org/10.1175/1520-0442(1992)005<0541:AIOMFF>2.0.CO;2.

Cadet, D.L., 1985. The southern oscillation over the indian ocean. J. Climatol. 5, 189–212. https://doi.org/10.1002/joc.3370050206.

Camberlin, P., Philippon, N., 2002. The East African March – May Rainy Season : Associated Atmospheric Dynamics and Predictability over the 1968–97 Period. J. Clim. 15, 1002–1019. https://doi.org/10.1175/1520-0442(2002)015%3C1002:TEAMMR%3E2.0.CO;2.

Epstein, P.R., 1999. Climate and health. Science (80-) 285, 347–348.

Fang, Y.H., Chen, H.S., Da Teng, F., et al., 2017. Changing contribution rate of heavy rainfall to the rainy season precipitation in Northeast China and its possible causes. Atmos. Res. 197, 437–445. https://doi.org/10.1016/j.atmosres.2017.07.030.

Fang, Y.H., Chen, K.-Q., Chen, H.-S., et al., 2018. The remote responses of early summer cold vortex precipitation in northeastern china compared with the previous sea surface temperatures. Atmos. Res. 214, 399–409. https://doi.org/10.1016/j.atmosres.2018.08.

Giannini, A., 2003. Oceanic Forcing of Sahel Rainfall on Interannual to Interdecadal Time Scales. Science (80-) 302, 1027–1030. https://doi.org/10.1126/science.1089357.

Goddard, L., Graham, N.E., 1999. Importance of the Indian Ocean for simulating rainfall anomalies over eastern and southern Africa. J. Geophys. Res. Atmos. 104, 19099–19116. https://doi.org/10.1029/1999JD900326.

Graham, N.E., Barnett, T.P., 1987. Sea Surface Temperature, Surface Wind Divergence, and Convection over Tropical Oceans. Science (80-) 238, 657–659. https://doi.org/10.1126/science.238.4827.657.

Hastenrath, S., 2007. Circulation mechanisms of climate anomalies in East Africa and the equatorial Indian Ocean. Dyn Atmos Ocean 43, 25–35. https://doi.org/10.1016/j.dynatmoce.2006.06.002.

Hastenrath, S., Nicklis, A., Greischar, L., 1993. Atmospheric-hydrospheric mechanisms of climate anomalies in the western equatorial Indian Ocean. J. Geophys. Res. 98, 20219. https://doi.org/10.1029/93JC02330.

Hills, R.C., 1978. The structure of the Inter-Tropical Convergence zone in Equatorial Africa and its relationship to East African rainfall. R Geogr Soc 4, 329–352. https://doi.org/10.2307/622055.

Hoskins, B.J., Hsu, H.H., James, I.N., Sardeshmurk, P.D., 1989. Diagnostics of the global atmospheric circulation based on ECMWF analysis 1979–1989. In: World Meteorol Organ Tech Rep WMO/TD-326 WCRP-27:217.

Indeje, M., Semazzi, F.H.M., Ogallo, L.J., 2000. ENSO signals in East African rainfall seasons. Int. J. Climatol. 20, 19–46. https://doi.org/10.1002/(SICI)1097-0088(200001)20:1<19::AID-JOC449>3.0.CO;2-0.

Jiang, X., Waliser, D.E., Olson, W.S., et al., 2011. Vertical Diabatic heating Structure of the MJO: Intercomparison between recent Reanalyses and TRMM estimates. Mon. Weather Rev. 139, 3208–3223. https://doi.org/10.1175/2011MWR3636.1.

Jiang, X., Yang, S., Li, Y., et al., 2013. Dominant modes of wintertime upper-tropospheric temperature variations over Asia and links to surface climate. J. Clim. 26, 9043–9060. https://doi.org/10.1175/JCLI-D-12-00774.1.

Kalnay, E., Kanamitsu, M., Kistler, R., et al., 1996. The NCEP/NCAR 40-year reanalysis project. Bull. Am. Meteorol. Soc. 77, 437–471.

Latif, M., Dommenget, D., Dima, M., Grötzner, A., 1999. The role of Indian Ocean Sea surface temperature in forcing east African rainfall anomalies during December-January 1997/98. J. Clim. 12, 3497–3504. https://doi.org/10.1175/1520-0442(1999)012<3497:TROIOS>2.0.CO;2.

Liebmann, B., Smith, C.A., 1996. Description of a complete (interpolated) outgoing longwave radiation dataset. Bull. Am. Meteorol. Soc. 77, 1275–1277.

Lindzen, R.S., Nigam, S., 1987. On the Role of Sea Surface Temperature Gradients in Forcing Low-Level Winds and Convergence in the Tropics. J. Atmos. Sci. 44, 2418–2436.

Mafuru, K.B., Guirong, T., 2018. Assessing Prone areas to Heavy Rainfall and the Impaction of the Upper warm Temperature Anomaly during March-May Rainfall season in Tanzania. Adv. Meteorol. 2018. https://doi.org/10.1155/2018/8353296.

Mafuru, K.B., Tan, G., 2019. The influence of ENSO on the upper warm temperature anomaly formation associated with the March–May heavy rainfall events in Tanzania. Int J Climatol 1–19. https://doi.org/10.1002/joc.6364.

Mutai, C.C., Ward, M.N., 2000. East African rainfall and the tropical circulation/convection on intraseasonal to interannual timescales. J. Clim. 13, 3915–3939. https://doi.org/10.1175/1520-0442(2000)013<3915:EARATT>2.0.CO;2.

Nguyen, H., Duvel, J.P., 2008. Synoptic wave perturbations and convective systems over equatorial Africa. J. Clim. 21, 6372–6388. https://doi.org/10.1175/2008JCLI2409.1.

Nigam, S., 1994. On the dynamical basis for the Asian summer monsoon rainfall–El Nino relationship. J. Clim. 7, 1750–1771.

Ogallo, L.J., 1988. Relationships between seasonal rainfall in East Africa and the Southern Oscillation. J. Climatol. 8, 31–43. https://doi.org/10.1002/joc.3370080104.

Ogallo, L.J., Janowiak, J.E., Halpert, M.S., 1988. Teleconnection between seasonal rainfall over East Africa and global sea surface temperature anomalies. J Meteorol Soc Japan 66, 807–821.

Okoola, R.E., 1989. Westwards moving disturbances in the Southwest Indian Ocean. Meteorog. Atmos. Phys. 41, 35–44. https://doi.org/10.1007/BF01032588.

Phillips, J., McIntyre, B., 2000. ENSO and interannual rainfall variability in Uganda: implications for agricultural management. Int. J. Climatol. 20, 171–182. https://doi.org/10.1002/(SICI)1097-0088(200002)20:2<171::AID-JOC471>3.0.CO;2-O.

Preethi, B., Sabin, T.P., Adedoyin, J.A., Ashok, K., 2015. Impacts of the ENSO Modoki and other tropical indo-pacific climate- drivers on african rainfall. Nat Publ Gr 1–15. https://doi.org/10.1038/srep16653.

Raymond, D.J., 1994. Convective processes and tropical atmospheric circulations. Q. J. R. Meteorol. Soc. 120, 1431–1455. https://doi.org/10.1002/qj.49712052002.

Reverdin, G., Cadet, D.L., Gutzler, D., 1986. Interannual displacements of convection and surface circulation over the equatorial Indian Ocean. Q. J. R. Meteorol. Soc. 112, 43–67. https://doi.org/10.1002/qj.49711247104.

Roundy, P.E., 2008. Analysis of Convectively coupled Kelvin Waves in the Indian Ocean MJO. J. Atmos. Sci. 65, 1342–1359. https://doi.org/10.1175/2007JAS2345.1.

Roundy, P.E., 2015. On the interpretation of EOF analysis of ENSO, atmospheric Kelvin waves, and the MJO. J. Clim. 28, 1148–1165. https://doi.org/10.1175/JCLI-D-14-00398.1.

Rowell, D.P.,Ininda, J.M., MNW, 1994. The impact of global sea surface temperature patterns on seasonal rainfall in East Africa. In: Proc. Int. Conf. on Monsoon Variability and Prediction. WMO, Trieste, Italy, pp. 666–672.

Smith, T.M., Reynolds, R.W., Peterson, T.C., Lawrimore, J., 2008. Improvements to NOAA's historical merged land-ocean surface temperature analysis (1880-2006). J. Clim. 21, 2283–2296. https://doi.org/10.1175/2007JCLI2100.1.

Straub, K.H., Kiladis, G.N., 2002. Observations of a Convectively coupled Kelvin Wave in the Eastern Pacific ITCZ. J. Atmos. Sci. 59, 30–53. https://doi.org/10.1175/1520-0469(2002)059<0030:OOACCK>2.0.CO;2.

Tamura, T., Taniguchi, K., Koike, T., 2010. Mechanism of upper tropospheric warming around the Tibetan Plateau at the onset phase of the Asian summer monsoon. J. Geophys. Res. Atmos. 115. https://doi.org/10.1029/2008JD011678.

Ummenhofer, C.C., Sen, Gupta A., England, M.H., CJC, Reason, 2009. Contributions of Indian Ocean Sea surface temperatures to enhanced East African rainfall. J. Clim. 22, 993–1013. https://doi.org/10.1175/2008JCLI2493.1.

Verdin, J., Funk, C., Senay, G., Choularton, R., 2005. Climate science and famine early warning. Philos Trans R Soc B Biol Sci 360, 2155–2168. https://doi.org/10.1098/rstb.2005.1754.

Viste, E., Korecha, D., Sorteberg, A., 2013. Recent drought and precipitation tendencies in Ethiopia. Theor. Appl. Climatol. 112, 535–551. https://doi.org/10.1007/s00704-012-0746-3.

Wheeler, M., Kiladis, G.N., 1999. Convectively coupled Equatorial Waves: Analysis of Clouds and Temperature in the Wavenumber–Frequency Domain. J. Atmos. Sci. 56, 374–399. https://doi.org/10.1175/1520-0469(1999)056<0374:CCEWAO>2.0.CO;2.

Wheeler, M., Kiladis, G.N., Webster, P.J., 2000. Large-Scale Dynamical Fields Associated with Convectively coupled Equatorial Waves. J. Atmos. Sci. 57, 613–640. https://doi.org/10.1175/1520-0469(2000)057<0613:LSDFAW>2.0.CO;2.

Yanai, M., Li, C.F., 1994. Mechanism of heating and the Boundary-Layer over the Tibetan Plateau. Mon. Weather Rev. 122, 305–323.

Zhang, L., Zhou, T., 2012. The interannual variability of summer upper-tropospheric temperature over East Asia. J. Clim. 25, 6539–6553. https://doi.org/10.1175/JCLI-D-11-00583.1.